chemosensors

MDPI

Communication

Preparation and Enhanced Acetone-Sensing Properties of ZIF-8-Derived Co_3O_4@ZnO Microspheres

Xiangxiang Fan [1,2,*], Susu Yang [1], Chun Huang [1], Yujie Lu [1] and Pan Dai [1,2]

[1] School of Information Engineering, Huzhou University, Huzhou 313000, China; yangsusu2739@126.com (S.Y.)
[2] Zhejiang Province Key Laboratory of Smart Management & Application of Modern Agricultural Resources, Huzhou University, Huzhou 313000, China
* Correspondence: fanxiangxiang@zjhu.edu.cn

Abstract: In this work, ZIF-8-derived Co_3O_4@ZnO microspheres were prepared by a liquid-phase concentration-controlled nucleation strategy. The results of the material characterization showed that Co_3O_4@ZnO microspheres were obtained, and the surface structure could be controlled with the concentration of the ligand. Compared with pure Co_3O_4 microspheres, the operating temperature of optimized Co_3O_4@ZnO microspheres increased by 90 °C after the gas-sensing test. The response to 50 ppm acetone of Co_3O_4@ZnO microspheres was 4.5 times higher than that of pure Co_3O_4, and the detection limit reached 0.5 ppm. Meanwhile, Co_3O_4@ZnO microspheres showed a shorter response-recovery time and better selectivity. The enhanced-sensing mechanism of the ZIF-8-derived Co_3O_4@ZnO microspheres was also analyzed.

Keywords: gas sensor; microspheres; MOF; ZIF-8

Citation: Fan, X.; Yang, S.; Huang, C.; Lu, Y.; Dai, P. Preparation and Enhanced Acetone-Sensing Properties of ZIF-8-Derived Co_3O_4@ZnO Microspheres. *Chemosensors* **2023**, *11*, 376. https://doi.org/10.3390/chemosensors11070376

Academic Editor: Manuel Aleixandre

Received: 9 June 2023
Revised: 30 June 2023
Accepted: 3 July 2023
Published: 5 July 2023

1. Introduction

Acetone is not only an important organic solvent but also a respiratory marker of diabetes. The concentration of acetone in the exhaled breath of a diabetic patient is 1.8 ppm, while the concentration for a healthy person is less than 0.9 ppm. In order to diagnose diabetes, it is of great significance to prepare an acetone sensor with a detection limit of the ppb level [1]. Due to the advantages of their small size, low cost, and easy preparation [2,3], metal-oxide semiconductor (MOS) gas sensors have been widely used for acetone detection, such as In_2O_3, SnO_2, and Co_3O_4 [4–6]. Compared with the n-type MOS, previous studies have shown that Co_3O_4-based sensors exhibited the features of lower working temperature and higher selectivity [7,8]. Co_3O_4 is considered a promising MOS material for acetone-sensing with low power consumption. The response to 200 ppm acetone of Co_3O_4 nanoparticles prepared by Zhang et al. was 2.6 at 190 °C [9]. Park et al. synthesized Co_3O_4 hollow microspheres, and the response to 1000 ppm acetone was 7.5 at 100 °C [10]. However, the application of pure Co_3O_4-based sensors is still limited by their low sensitivities.

To obtain improved gas-sensing properties of Co_3O_4-based sensors, a general method is to prepare heterojunctions. The response to 50 ppm acetone of Co_3O_4/ZnO heterogeneous material prepared by Zhao's team was approximately 5.1 times higher than the value of pure Co_3O_4 [11]. The response to 5 ppm TMA of Co_3O_4/SnO_2 heterogeneous material prepared by Meng's team was 7.2 times higher than the value of pure Co_3O_4 [12]. Therefore, enhanced sensing properties can be obtained by constructing a heterojunction. The structures of heterogeneous materials include a hybrid heterostructure, a decorated heterostructure, and a multilayer heterostructure [13–16]. Among them, the decorated heterostructure is beneficial for gas sensing due to its good synergistic effect between the core and shell components and larger heterointerface [17,18]. The response to 100 ppm formaldehyde of In_2O_3@SnO_2 heterostructure Nanofibers prepared by Wan et al. was higher than that of pure In_2O_3 Nanofibers and pure SnO_2 nanosheets [19]. A variety of

decorated heterostructures have been reported as sensing materials, such as In_2O_3@NiO, CeO_2@$ZnSnO_3$, and Co_3O_4@WO_3 [20–22]. All the reported decorated heterostructures have shown improved gas-sensing properties.

Metal-organic framework (MOF) materials, with their large specific surface area and high porosity, have shown great value for application in the fields of gas storage, energy storage, adsorption, and catalysis [23–25]. Since the porous MOS structure can be obtained via heating treatment, MOF materials have received extensive attention for the preparation of sensors [26–28]. More gas adsorption and reaction sites in porous MOS could significantly enhance the gas-sensing properties [29]. Therefore, more attention has been paid to the decorated heterostructures prepared by MOF. As a representative MOF material, ZIF-8 is bridged by 2-methylimidazole and Zn^{2+}. ZnO could be obtained by annealing treatment of ZIF-8. The material of ZnO exhibits high charge-carrier mobility and high sensitivity [30,31], and ZIF-8-derived ZnO obtained extensive attention as a gas sensor. The response to 500 ppb acetone of ZIF-8-derived ZnO@MoS_2 heterostructures prepared by Chang's group reached 1.5 at 350 °C [32]. Zhan et al. prepared ZIF-8-derived SnO_2@ZnO microspheres, which showed a response of 164 to 70 ppm NO_2 at 300 °C [33]. The excellent gas-sensing performances benefit from the heterojunction and porous structure. However, these ZIF-8-derived n-type ZnO heterogeneous materials were always operated at a high temperature. As a sensing material with low power consumption, Co_3O_4 with ZIF-8-derived ZnO coating was rarely reported.

In this work, ZIF-8-derived Co_3O_4@ZnO microspheres were prepared using the liquid-phase concentration-controlled nucleation strategy. The surface structure was controlled with the concentration of the ligand. The acetone-sensing properties and mechanism of the heterostructure were analyzed.

2. Materials and Methods

2.1. Materials

2-methylimidazole (2-MeIM, AR), zinc acetate ($Zn(COOH_3)_2{\cdot}2H_2O$, AR), cobalt nitrate hexahydrate ($Co(NO_3)_2{\cdot}6H_2O$, AR), sodium hydroxide (NaOH, AR), ethanol (CH_3CH_2OH, AR), and methanol (CH_3OH, AR) were all bought from Aladdin (Shanghai, China). All the reagents were utilized without pretreatment.

2.2. Synthesis of Co_3O_4 Microspheres

First, 58.21 g $Co(NO_3)_2{\cdot}6H_2O$ was added to 40 mL deionized water to obtain a purple solution, then 2 g NaOH was added and stirred for 10 min. Second, the supernatant of the solution was transferred into a 50 mL Teflon-lined autoclave and kept at 180 °C for 5 h. After the reaction, the precipitate was obtained by centrifugation. The precipitate was washed with ethanol and water three times, and the Co_3O_4 precursor was obtained after being dried at 70 °C for 3 h. Finally, Co_3O_4 microspheres were obtained by calcining the precursor at 500 °C for 2 h.

2.3. Synthesis of Co_3O_4@ZnO Microspheres

Solution A was obtained by dissolving 0.0714 g $Zn(COOH_3)_2{\cdot}2H_2O$ in 10 mL of methanol. Solution B was obtained by dissolving a certain amount of 2-methylimidazole and 50 mg of the Co_3O_4 precursor in 10 mL of methanol, followed by sonication for 1 h. Solutions A and B were mixed and stirred for 30 min. After standing for 24 h, the precipitate was obtained by centrifugation. The precipitate was washed with ethanol and water three times, and the precursor of Co_3O_4@ZnO microspheres was obtained after being dried at 60 °C for 12 h. After being annealed at 500 °C for 3 h, Co_3O_4@ZnO microspheres were obtained.

The amount of 2-MeIM added was set as 3.7 times, 37 times, and 110 times that of the molar amount of Zn^{2+}, and the corresponding materials were named CZ-1, CZ-2, and CZ-3.

2.4. Material Characterization

Scanning electron microscopy (SEM, Apreo 2S, ThermoFischer, Waltham, MA, USA) and transmission electron microscopy (TEM, Talos F200S G2, ThermoFischer) were utilized to characterize the morphology and surface structure of the materials. The element compositions were analyzed by energy-dispersive X-ray spectroscopy (EDS, QUANTAX EDS, Bruker, Billerica, MA, USA). The crystal composition and crystallinity were analyzed by X-ray diffraction spectroscopy (XRD, Ultima IV, Rigaku, Tokyo, Japan). X-ray photoelectron spectroscopy (XPS, ESCALAB Xi+, ThermoFischer) was utilized to characterize the chemical ingredients and states of the samples.

2.5. Preparation and Measurement of Sensors

The fabrication method of the sensors is consistent with our previous report [34]. Specifically, 10 mg of Co_3O_4@ZnO microspheres were mixed with 100 µL of ethanol to obtain the homogeneous paste, and it was evenly brushed onto the outer surface of a ceramic tube equipped with a Cr-Ni heating wire and a pair of gold electrodes. After being annealed at 300 °C for 12 h, the acetone sensor was obtained.

As shown in Figure 1, the test system includes a humidity generator, a test chamber, and a source meter. The humidity generator is used to generate different humidity environments. The air was filtered and passed through a saturated salt solution by an air pump. When the air was introduced into the test chamber, the environment with the required humidity was obtained and the relative humidity was determined by a humidity sensor. The measurement of our sensor was performed in an 18 L test chamber whose size was 300 mm × 300 mm × 200 mm. A source meter was used to record the data.

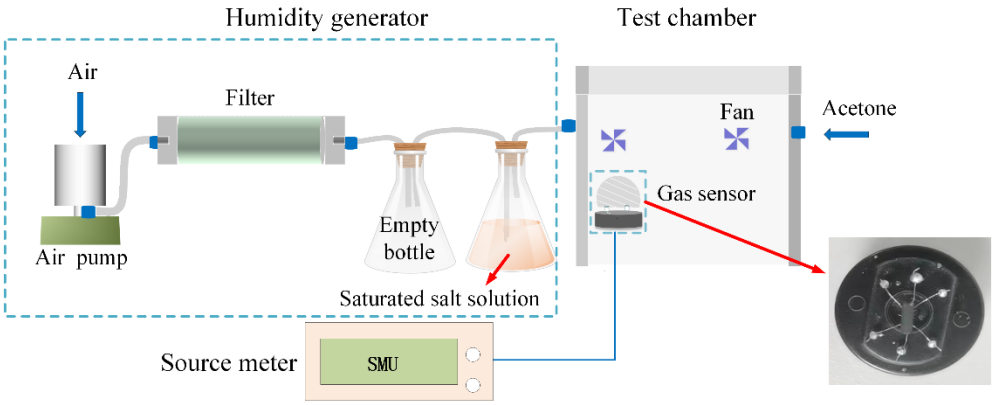

Figure 1. Schematic diagram of gas-sensing test system.

Gas-sensing properties were analyzed by injecting saturated acetone vapor into the test chamber or exhausting acetone from the chamber as per our previous report [35]. When acetone gas was injected, the gas was stirred evenly by the fans. The concentration of acetone is adjusted by changing the volume of saturated steam injected into the chamber [36]. The concentration could be calculated by the formula $C_g = V_g P_g / P_0 V_c$, where V_g is the volume of acetone injected into the chamber, P_g is the saturated vapor pressure of acetone, P_0 is the ambient atmospheric pressure, and V_c is the volume of the test chamber. After the test, the acetone gas in the test chamber was replaced with fresh air through the air pump.

The ratios of $(R_g - R_a)/R_a$ were used to describe the sensitivity of the sensors, where R_g and R_a are the resistances of the sensors in target gas and air. The times required to change the resistance by 90% after injecting or exhausting the target gas were used to define the response and recovery time.

3. Results

3.1. Materials Characterization

Figure 2a presents that the Co_3O_4 particle is a spherical structure with a smooth surface, and the size is approximately 300 nm. As shown in Figure 2b–d, all the samples of CZ-1, CZ-2, and CZ-3 still maintain spherical structures, but the surface characteristics have undergone dramatic changes. With the increase in the 2-methimidazole concentration, Co_3O_4 microspheres are gradually covered by nanoparticles, and the surfaces become rougher when the number of covered grains gradually increased. Therefore, the microspheres with decorated particles can be prepared by this method, and the surface structure can be adjusted by changing the ligand concentration.

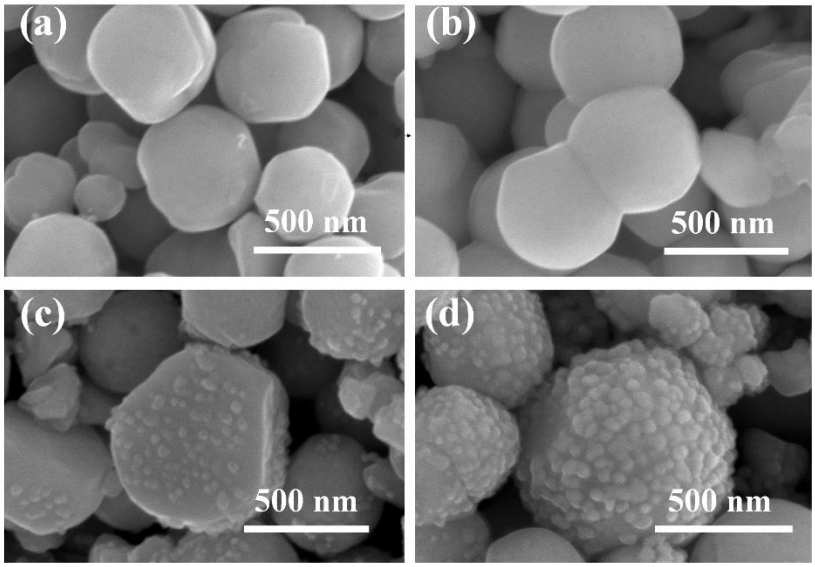

Figure 2. SEM images of (**a**) Co_3O_4, (**b**) CZ-1, (**c**) CZ-2, and (**d**) CZ-3.

The XRD spectra of Co_3O_4, CZ-1, CZ-2, and CZ-3 are displayed in Figure 3. The peaks of Co_3O_4 are located at 31.24°, 36.82°, 44.78°, 55.66°, and 59.22°, which correspond to (2 2 0), (3 1 1), (4 0 0), (4 2 2), and (5 1 1) crystal planes of spinel Co_3O_4 (JCPDS No.43-1003). The spectra of CZ-1, CZ-2, and CZ-3 also show identical diffraction peaks of Co_3O_4, indicating that Co_3O_4 crystal is formed in these samples. On the XRD spectrum of CZ-3, three different diffraction peaks are formed from other samples, which are located at 31.6°, 36.24°, and 56.42°. These peaks are indexed to the (1 0 0), (1 0 1), and (1 1 0) crystal planes of ZnO. The results indicate that the CZ-3 contains crystals of Co_3O_4 and ZnO. However, due to the low content of ZnO, the three peaks are not observed on the spectra of CZ-1 and CZ-2.

As shown in Figure 4, all the samples were further analyzed by TEM and EDS to confirm the morphologies and compositions. Figure 4a,b present that pure Co_3O_4 and CZ-1 are both smooth microspheres. Figure 4c,d exhibit that the Co_3O_4 microspheres are coated by ZnO nanoparticles and the amount of ZnO nanoparticles gradually increases with the increase in the 2-methimidazole concentration. In order to verify that CZ-1 is coated by ZnO, EDS was used to analyze the element on the surface. Figure 4e,f show that the element of Zn is evenly distributed on the surface of Co_3O_4 microspheres. The smooth surface of CZ-1 can contribute to the small size of ZnO nanoparticles. Figure 4g,h indicate that the main element in the nanoparticles coated on the microspheres is Zn. Figure 4i shows that the lattice width of the nanoparticles coated on the microspheres is 0.26 nm and is indexed to the (0 0 2) crystal plane of ZnO. The results indicate that Co_3O_4@ZnO microspheres are obtained by the liquid-phase concentration-controlled nucleation strategy.

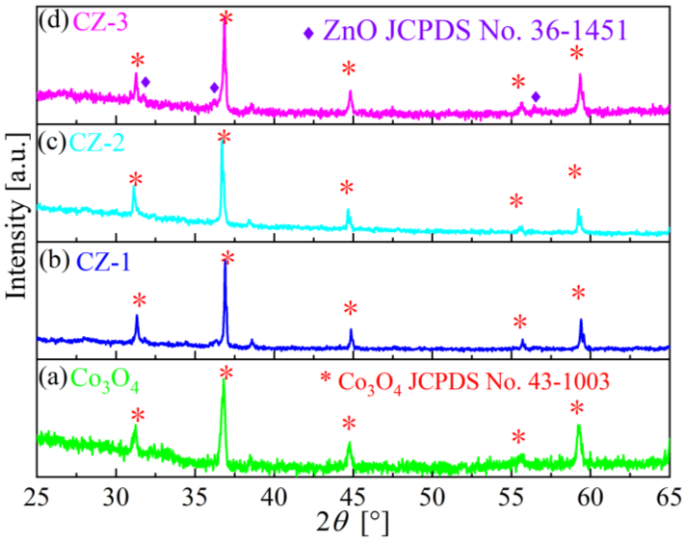

Figure 3. XRD spectra of (**a**) Co_3O_4, (**b**) CZ-1, (**c**) CZ-2, and (**d**) CZ-3.

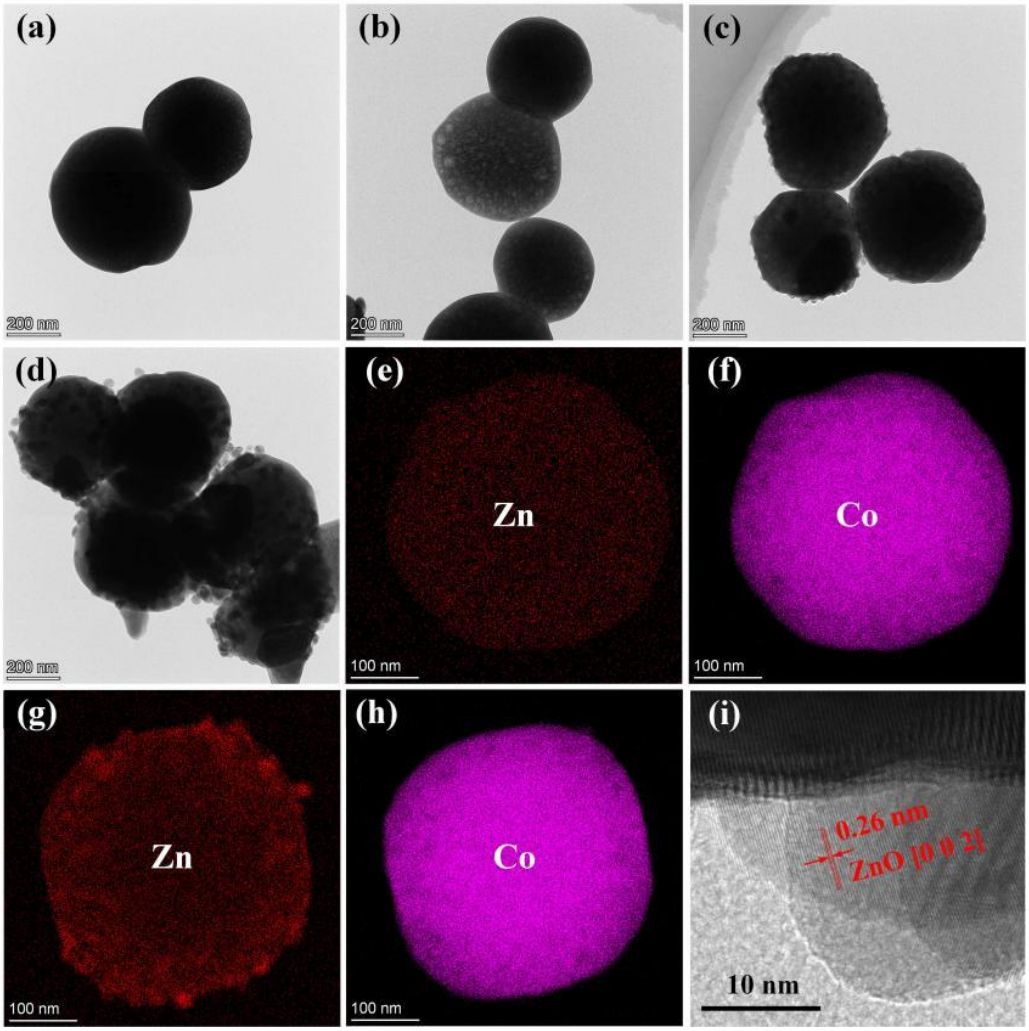

Figure 4. TEM images of (**a**) Co_3O_4, (**b**) CZ-1, (**c**) CZ-2m and (**d**) CZ-3. EDS mapping images of (**e**,**f**) CZ-1 and (**g**,**h**) CZ-2. (**i**) HRTEM images of CZ-2.

Figure 5a shows that the elements of Zn, O, and Co are presented on the XPS spectrum of CZ-2, while only Co and O appear in Co_3O_4. Figure 5b shows the high-resolution

XPS spectrum of Zn 2p in CZ-2, which includes two peaks corresponding to Zn^{2+} [37]. Therefore, it is further proved that the nanograins coated on Co_3O_4 microspheres are ZnO. Figure 5c presents the Co 2p spectra of Co_3O_4 and CZ-2. The fitting peaks located at 797 eV and 782.5 eV are associated with Co^{2+}, while the fitting peaks located at 795 eV and 779.5 eV correspond to Co^{3+}. This demonstrates the existence of Co_3O_4 particles in the samples [38]. Figure 5d presents the O 1 s spectra of Co_3O_4 and CZ-2. The three different fitting peaks are related to lattice oxygen (O_L), oxygen vacancies (O_V), and absorbed oxygen (O_C) [39]. Among these, O_V is the key component to affect the gas-sensing performance. The gas-sensing property is attributed to the redox reaction between the target gas with oxygen adsorbed on the surface of the sensing material. As the donor, the oxygen vacancies provide sites for oxygen adsorption and reaction [40]. The area ratio O_V in Co_3O_4 is 29.8%, while that in CZ-2 is 39.1%. The O_V proportion of CZ-2 is higher than that of pure Co_3O_4.

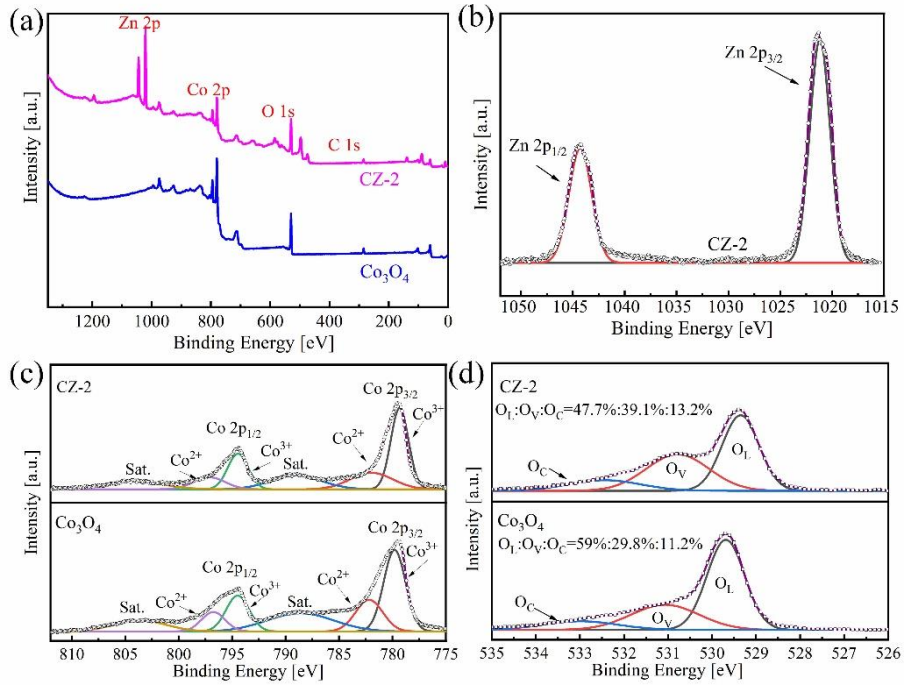

Figure 5. XPS spectra of (**a**) full survey for CZ-2 and Co_3O_4. High-resolution XPS spectra of (**b**) Zn 2p, (**c**) Co 2p, and (**d**) O 1 s.

3.2. Gas-Sensing Properties

The sensing properties of the material are always affected by the operating temperature. Figure 6a shows the resistances of four samples in the air at a temperature ranging from 130 °C to 280 °C. The resistance of all the samples decreases significantly as the temperature increases. Because of the heterojunctions, the resistance of Co_3O_4@ZnO microspheres is higher than that of pure Co_3O_4. The resistance of CZ-2 and CZ-3 even exceeds the range of the source meter at temperatures lower than 190 °C, making it impossible to accurately measure the resistance values. Figure 6b shows the responses of four sensors to 50 ppm acetone, operated at a temperature ranging from 130 °C to 280 °C. Co_3O_4, CZ-1, CZ-2, and CZ-3 reach the maximum response at 160 °C, 190 °C, 250 °C, and 250 °C. The optimal operating temperatures of all the Co_3O_4@ZnO microspheres are higher than the value of pure Co_3O_4 because of the presence of n-type MOS. Among them, CZ-2 shows the highest response at 250 °C, and the resistance in the air is approximately 600 kΩ. The response value of CZ-2 is 4.5 times higher than the value of pure Co_3O_4. Therefore, the acetone sensitivity of Co_3O_4 is enhanced by the ZIF-8-derived ZnO.

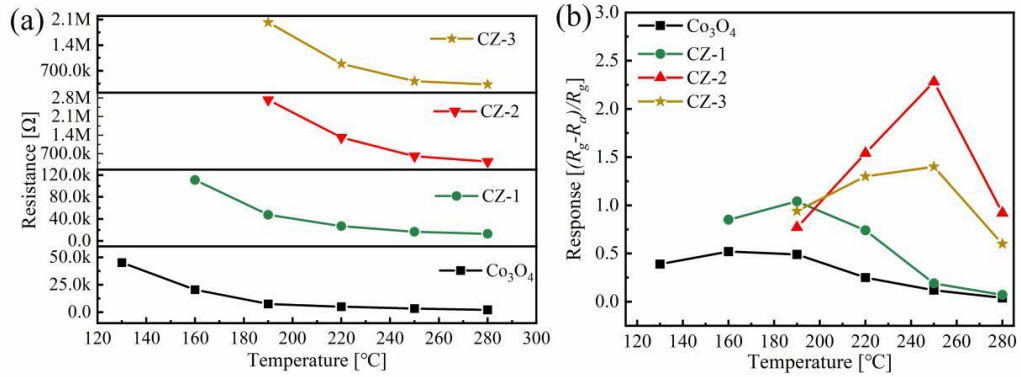

Figure 6. (**a**) Resistances in air and (**b**) responses to 50 ppm acetone of four samples at different operating temperatures.

The responses of pure Co_3O_4 and CZ-2 to 0.5–100 ppm acetone at the optimal operating temperature are displayed in Figure 7a. The response values of CZ-2 are larger than the values of Co_3O_4. Compared with pure Co_3O_4, the detection limit of CZ-2 reaches 500 ppb. As shown in Figure 7b, the response and recovery times of CZ-2 are 32 s and 98 s, which are shorter than that of pure Co_3O_4. Therefore, the sensitivity and response-recovery rates of Co_3O_4 are improved by the ZIF-8-derived ZnO.

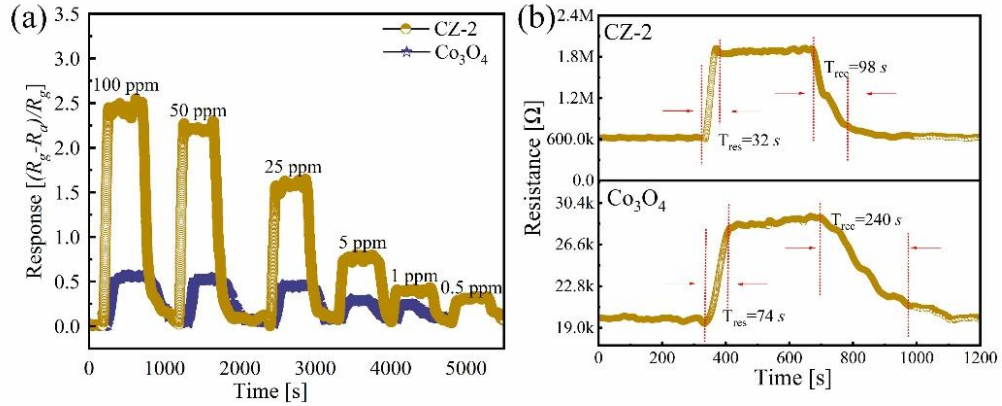

Figure 7. (**a**) Dynamic response curves of pure Co_3O_4 and CZ-2 to 0.5–100 ppm acetone. (**b**) Response-recovery curves of pure Co_3O_4 and CZ-2 to 50 ppm acetone.

As shown in Figure 8a, the responses of pure Co_3O_4 and CZ-2 to 50 ppm of different gases were tested at the optimized temperatures. The two samples show the highest response to acetone, which means that the two sensors have a selective response to acetone. To quantitatively investigate the selectivity of the two sensors, the ratios of $S_{others}/S_{acetone}$ are used and listed in Figure 8b, where $S_{acetone}$ and S_{others} are the responses of the sensor to acetone and other gas. Figure 8b presents that CZ-2 has lower ratios than pure Co_3O_4, which means that CZ-2 has better selectivity. According to the ratios, the selectivity of the sensor depends on the sensitivity of different gases, and the sensitivity of different gases is related to the reaction intensity of the gas on the surface of the sensing material. Due to the reaction intensity being influenced by the amount of adsorbed gas on the surface and the reaction energy, the material composition and working temperature are key factors to determine the selectivity, and the sensor exhibits the highest reaction intensity at the optimal operating temperature [13]. Compared with Co_3O_4, the acetone reaction intensity on the surface of CZ-2 is enhanced more than other gases, resulting in improved selectivity. The results show that the selectivity of Co_3O_4 is enhanced by ZIF-8-derived ZnO.

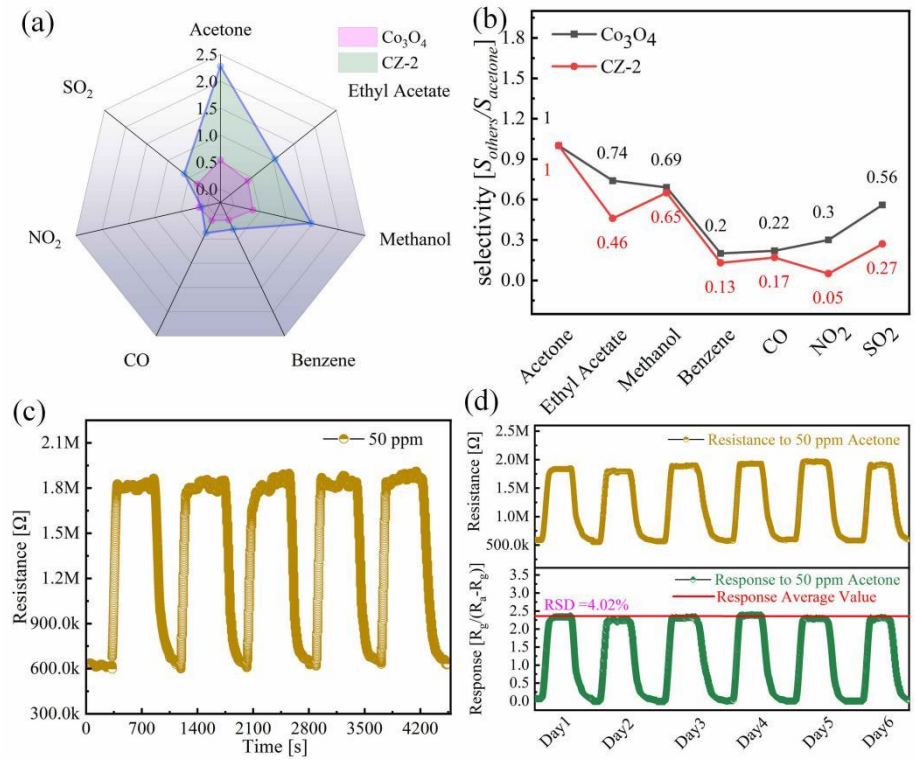

Figure 8. (**a**) Response to 50 ppm different gases and (**b**) ratios ($S_{others}/S_{acetone}$) of pure Co_3O_4 and CZ-2. (**c**) Cycle response curves and (**d**) response curves of CZ-2 during 6 days to 50 ppm acetone.

In order to evaluate the stability of the sensor, the multi-cycle tests of CZ-2 to 50 ppm acetone are shown in Figure 8c. The response curves of CZ-2 remain stable during the multi-cycle tests. The response curves of CZ-2 to 50 ppm acetone over 6 days are presented in Figure 8d. The responses of CZ-2 remain stable, and the relative standard deviation is 4.02%. The results exhibit that Co_3O_4@ZnO microspheres display good stability.

The response to acetone of CZ-2 was also investigated in an environment of relative humidity (RH) ranging from 30% to 80%. In order to quantitatively evaluate the anti-humidity property of CZ-2, the ratios of S_{others}/S_{30} were used as a comparative quantity, where S_{30} and S_{others} are the response in the environment of 30% RH and other RH. Figure 9 shows the ratios of CZ-2 as a function of relative humidity. As the humidity increased from 30% to 80%, the response of the CZ-2 decreased by 31% compared to the original. When the sensor is in a high-humidity environment, water molecules will adsorb on the surface of sensing materials and react with oxygen ions. A hydroxyl group with less activity is generated, and the sensitivity of the sensor decreases [41].

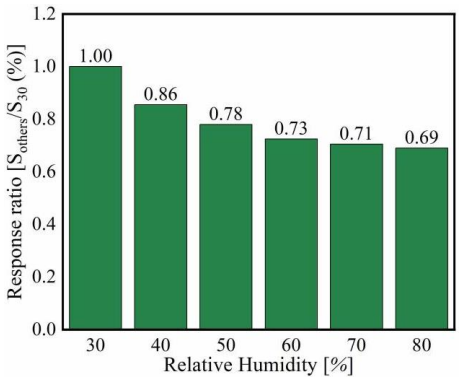

Figure 9. Response ratios (S_{others}/S_{30}) of CZ-2 as a function of relative humidity.

The acetone-sensing properties of different Co_3O_4-based sensors in this work and the previous reports are listed in Table 1 [42–46]. The ZIF-8-derived Co_3O_4@ZnO microspheres exhibit better sensitivity and a lower detection limit compared with the previous reports.

Table 1. Comparison of the gas-sensing performances of Co_3O_4-based sensors to acetone.

Material	Operating Temperature	Response	Detection Limit	References
Co_3O_4 rectangular rods	200 °C	1.94 (50 ppm)	5 ppm	[42]
Co_3O_4/Fe_2O_3 hollow cubes	250 °C	2.27 (100 ppm)	1 ppm	[43]
$Co_3O_4/NiCo_2O_4$ nanocages	238.9 °C	2.09 (100 ppm)	-	[44]
PdO-Co_3O_4 hollow Nanocages	350 °C	1.51 (5 ppm)	0.1 ppm	[45]
$Co_3O_4/ZnSnO_3$ nanorod array	250 °C	2.61 (100 ppm)	-	[46]
Co_3O_4@ZnO microspheres	250 °C	2.3 (50 ppm)	0.5 ppm	This work

4. Discussion

The sensing mechanism of MOS is similar to the description of the previous report [47]. As shown in Figure 10a, when Co_3O_4 is in the air environment, the electrons in the material are captured by the absorbed oxygen molecules to form oxygen ions. A hole-accumulating layer is formed on the surface of the material [48]. The adsorption processes of oxygen are expressed by Formulas (1)–(3). As shown in Figure 10b, when Co_3O_4 is in acetone, the acetone molecules react with the oxygen ions and electrons are released into the sensing material. The reaction processes between oxygen ions with acetone molecules are expressed by Formulas (4) and (5). Due to the reaction, the hole-accumulating layer becomes narrow. For the sensing material of Co_3O_4, the accumulation layer is a conducting channel, and a change in the accumulation layer directly affects the response value.

$$O_2(gas) \rightarrow O_2(ads) \quad (1)$$

$$O_2(ads) + e^- \rightarrow O_2{}^-(ads) \quad (2)$$

$$O_2{}^-(ads) + e^- \rightarrow 2O^-(ads) \quad (3)$$

$$CH_3COCH_3(gas) + 4O_2{}^-(ads) \rightarrow 3H_2O(gas) + 3CO_2(gas) + 4e^- \quad (4)$$

$$CH_3COCH_3(gas) + 8O^-(ads) \rightarrow 3CO_2(gas) + 3H_2O(gas) + 8e^- \quad (5)$$

As the test results show, ZIF-8-derived Co_3O_4@ZnO microspheres present a p-type semiconductor behavior. The improved acetone-sensing properties of CZ-2 contribute to the formed p-n heterojunction between ZnO with Co_3O_4, the increased oxygen vacancy of material, and the porous structure of MOF-derived ZnO.

Firstly, the formed p-n heterojunction between ZnO and Co_3O_4 is the key reason for the enhanced gas sensitivity. As Figure 10c,d show, the band gaps of ZnO and Co_3O_4 are 3.37 eV and 1.6 eV. When they are in contact, the carrier flows between ZnO with Co_3O_4 to make the Fermi level equilibrium. The depletion layers are formed on the interface of two materials, and the resistance primarily depends on the width of the depletion layer. When the sensor is in the air, the reactions of Formulas (1)–(3) occur on the Co_3O_4@ZnO microspheres. The electrons flowing from ZnO to Co_3O_4 decrease, which causes a decrease in the width of the hole-depleting layer on the Co_3O_4 side [49]. When acetone gas is introduced, the reactions of Formulas (4) and (5) occur on the material, leading to the hole-depleting layer increasing. For the Co_3O_4@ZnO microspheres, the resistance change rate caused by the depletion layer is significant, leading to higher sensitivity. Secondly, oxygen vacancy is an active site, which provides a venue for oxygen adsorption and reaction [40]. From XPS characterization, it is clear that the O_V component of CZ-2 is higher than that of

pure Co_3O_4. This indicates that more sites of oxygen adsorption and reaction are present on the surface of Co_3O_4@ZnO microspheres. Finally, the porous structure derived by ZIF-8 is also a favorable channel for acetone gas transmission. With the porous structure, the gas reaches the interface of the heterojunction more easily. Therefore, the acetone-sensing properties of Co_3O_4@ZnO microspheres are improved.

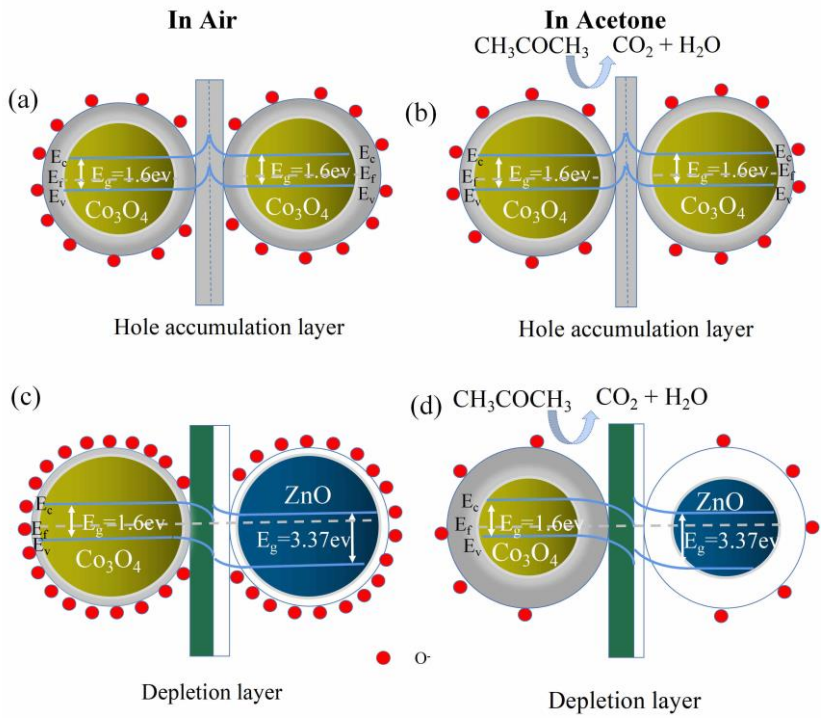

Figure 10. Schematic diagram of energy band structure of (**a**) pure Co_3O_4 in air, (**b**) pure Co_3O_4 in acetone, (**c**) Co_3O_4@ZnO in air and (**d**) Co_3O_4@ZnO in acetone.

5. Conclusions

ZIF-8-derived Co_3O_4@ZnO microspheres were prepared by a liquid-phase concentration-controlled nucleation strategy. This work indicated that the ZIF-8-derived surface structure could be controlled by changing the ligand concentration. Compared with pure Co_3O_4, the Co_3O_4@ZnO microspheres presented improved acetone-sensing properties. The sensor presents higher sensitivity, a faster response-recovery rate, and better selectivity and stability. This work shows that the preparation of an MOF-derived heterostructure is an effective way to enhance the gas-sensing performance of MOS materials.

Author Contributions: Conceptualization, X.F.; methodology, X.F. and P.D.; software, Y.L.; validation, X.F. and S.Y.; formal analysis, X.F. and C.H.; investigation, S.Y.; resources, Y.L.; data curation, S.Y. and C.H.; writing—original draft preparation, X.F. and S.Y.; writing—review and editing, X.F. and Y.L.; visualization, X.F. and S.Y.; supervision, X.F. and P.D.; project administration, X.F. and C.H.; funding acquisition, X.F. All authors have read and agreed to the published version of the manuscript.

Funding: This work was supported by the National Nature Science Foundation of China (No. 62201211).

Institutional Review Board Statement: Not applicable.

Informed Consent Statement: Not applicable.

Data Availability Statement: Not applicable.

Conflicts of Interest: The authors declare no conflict of interest.

References

1. Hanh, N.H.; Van Duy, L.; Hung, C.M.; Xuan, C.T.; Van Duy, N.; Hoa, N.D. High-Performance Acetone Gas Sensor Based on Pt–Zn_2SnO_4 Hollow Octahedra for Diabetic Diagnosis. *J. Alloys Compd.* **2021**, *886*, 161284. [CrossRef]
2. Isaac, N.; Pikaar, I.; Biskos, G. Metal Oxide Semiconducting Nanomaterials for Air Quality Gas Sensors: Operating Principles, Performance, and Synthesis Techniques. *Microchim. Acta* **2022**, *189*, 196. [CrossRef] [PubMed]
3. Yuan, Z.; Zhao, Q.N.; Xie, C.Y.; Liang, J.G.; Duan, X.H.; Duan, Z.H.; Li, S.R.; Jiang, Y.D.; Tai, H.L. Gold-Loaded Tellurium Nanobelts Gas Sensor for ppt-Level NO_2 Detection at Room Temperature. *Sens. Actuators B Chem.* **2022**, *355*, 131300. [CrossRef]
4. Kohli, N.; Hastir, A.; Kumari, M.; Singh, R.C. Hydrothermally Synthesized Heterostructures of In_2O_3/MWCNT as Acetone Gas Sensor. *Sens. Actuators A Phys.* **2020**, *314*, 112240. [CrossRef]
5. Kim, H.; Cai, Z.; Chang, S.-P.; Park, S. Improved Sub-ppm Acetone Sensing Properties of SnO_2 Nanowire-Based Sensor by Attachment of Co_3O_4 Nanoparticles. *J. Mater. Res. Technol.* **2020**, *9*, 1129–1136. [CrossRef]
6. Kumarage, G.W.; Comini, E. Low-Dimensional Nanostructures Based on Cobalt Oxide (Co_3O_4) in Chemical-Gas Sensing. *Chemosensors* **2021**, *9*, 197. [CrossRef]
7. Yusof, N.M.; Rozali, S.; Ibrahim, S.; Siddick, S.Z. Synthesis of Hybridized Fireworks-like go-Co_3O_4 Nanorods for Acetone Gas Sensing Applications. *Mater. Today Commun.* **2023**, *35*, 105516. [CrossRef]
8. Ramakrishnan, V.; Unnathpadi, R.; Pullithadathil, B. P-Co_3O_4 Supported Heterojunction Carbon Nanofibers for Ammonia Gas Sensor Applications. *J. Mater. Sci.* **2022**, *9*, 61–67.
9. Zhang, R.; Zhou, T.-T.; Wang, L.-L.; Zhang, T. Metal–Organic Frameworks-Derived Hierarchical Co_3O_4 Structures as Efficient Sensing Materials for Acetone Detection. *ACS Appl. Mater. Interfaces* **2018**, *10*, 9765–9773. [CrossRef]
10. Park, J.; Shen, X.P.; Wang, G.X. Solvothermal Synthesis and Gas-Sensing Performance of Co_3O_4 Hollow Nanospheres. *Sens. Actuators B Chem.* **2009**, *136*, 494–498. [CrossRef]
11. Zhao, L.P.; Jin, R.R.; Wang, C.; Wang, T.S.; Sun, Y.F.; Sun, P.; Lu, G.Y. Flower-like ZnO-Co_3O_4 Heterojunction Composites for Enhanced Acetone Sensing. *Sens. Actuators B Chem.* **2023**, *390*, 133964. [CrossRef]
12. Meng, D.; Si, J.P.; Wang, M.Y.; Wang, G.S.; Shen, Y.B.; San, X.G.; Meng, F.L. One-Step Synthesis and the Enhanced Trimethylamine Sensing Properties of Co_3O_4/SnO_2 Flower-like Structures. *Vacuum* **2020**, *171*, 108994. [CrossRef]
13. Fan, X.X.; Xu, Y.J.; He, W.M. High Acetone Sensing Properties of In_2O_3–NiO One-Dimensional Heterogeneous Nanofibers Based on Electrospinning. *RSC Adv.* **2021**, *11*, 11215–11223. [CrossRef]
14. Cai, Z.; Park, S. Highly Selective Acetone Sensor Based on Co_3O_4-Decorated Porous TiO_2 Nanofibers. *J. Alloys Compd.* **2022**, *919*, 165875. [CrossRef]
15. Karnati, P.; Akbar, S.; Morris, P.A. Conduction Mechanisms in One Dimensional Core-Shell Nanostructures for Gas Sensing: A Review. *Sens. Actuators B Chem.* **2019**, *295*, 127–143. [CrossRef]
16. Rehman, B.; Bhalla, N.K.; Vihari, S.; Jain, S.K.; Vashishtha, P.; Gupta, G. SnO_2/Au Multilayer Heterostructure for Efficient CO Sensing. *Mater. Chem. Phys.* **2020**, *244*, 122741. [CrossRef]
17. Xu, Y.S.; Zheng, L.L.; Yang, C.; Zheng, W.; Liu, X.H.; Zhang, J. Chemiresistive Sensors Based on Core-Shell ZnO@TiO_2 Nanorods Designed by Atomic Layer Deposition for N-Butanol Detection. *Sens. Actuators B Chem.* **2020**, *310*, 127846. [CrossRef]
18. Xu, Y.H.; Ding, L.J.; Wen, Z.R.; Zhang, M.; Jiang, D.; Guo, Y.S.; Ding, C.F.; Wang, K. Core-Shell $LaFeO_3$@G-C_3N_4 PN Heterostructure with Improved Photoelectrochemical Performance for Fabricating Streptomycin Aptasensor. *Appl. Surf. Sci.* **2020**, *511*, 145571. [CrossRef]
19. Wan, K.; Wang, D.; Wang, F.; Li, H.J.; Xu, J.C.; Wang, X.Y.; Yang, J.H. Hierarchical In_2O_3@SnO_2 Core–Shell Nanofiber for High Efficiency Formaldehyde Detection. *ACS Appl. Mater. Interfaces* **2019**, *11*, 45214–45225. [CrossRef]
20. Yan, S.; Song, W.N.; Wu, D.; Jin, S.C.; Dong, S.W.; Hao, H.S.; Gao, W.Y. Assembly of In_2O_3 Nanoparticles Decorated NiO Nanosheets Heterostructures and Their Enhanced Gas Sensing Characteristics. *J. Alloys Compd.* **2022**, *896*, 162887. [CrossRef]
21. Yu, S.W.; Jia, X.H.; Yang, J.; Wang, S.Z.; Li, Y.; Song, H.J. Highly Sensitive and Low Detection Limit of Ethanol Gas Sensor Based on CeO_2 Nanodot-Decorated $ZnSnO_3$ Hollow Microspheres. *Ceram. Int.* **2022**, *48*, 14865–14875. [CrossRef]
22. Gui, Y.H.; Yang, L.-L.; Tian, K.; Zhang, H.Z.; Fang, S.M. P-Type Co_3O_4 Nanoarrays Decorated on the Surface of N-Type Flower-like WO_3 Nanosheets for High-Performance Gas Sensing. *Sens. Actuators B Chem.* **2019**, *288*, 104–112. [CrossRef]
23. Felix Sahayaraj, A.; Joy Prabu, H.; Maniraj, J.; Kannan, M.; Bharathi, M.; Diwahar, P.; Salamon, J. Metal–Organic Frameworks (MOFs): The Next Generation of Materials for Catalysis, Gas Storage, and Separation. *J. Inorg. Organomet. Polym. Mater.* **2023**. [CrossRef]
24. Kavian, S.; Hajati, S.; Moradi, M. High-Rate Supercapacitor Based on NiCo-MOF-Derived Porous NiCoP for Efficient Energy Storage. *J. Mater. Sci. Mater. Electron.* **2021**, *32*, 13117–13128. [CrossRef]
25. Najafi, M.; Rahimi, R. Synthesis of Novel Zr-MOF/Cloisite-30B Nanocomposite for Anionic and Cationic Dye Adsorption: Optimization by Design-Expert, Kinetic, Thermodynamic, and Adsorption Study. *J. Inorg. Organomet. Polym. Mater.* **2023**, *33*, 138–150. [CrossRef]
26. Nair, S.S.; Illyaskutty, N.; Tam, B.; Yazaydin, A.O.; Emmerich, K.; Steudel, A.; Hashem, T.; Schöttner, L.; Wöll, C.; Kohler, H. ZnO@ZIF-8: Gas Sensitive Core-Shell Hetero-Structures Show Reduced Cross-Sensitivity to Humidity. *Sens. Actuators B Chem.* **2020**, *304*, 127184. [CrossRef]
27. Liu, C.Q.; Li, D.W.; Tang, W. Enhanced Ethanol Sensors Based on MOF-Derived ZnO/Co_3O_4 Bimetallic Oxides with High Selectivity and Improved Stability. *Vacuum* **2023**, *214*, 112185. [CrossRef]

28. Arul, C.; Moulaee, K.; Donato, N.; Iannazzo, D.; Lavanya, N.; Neri, G.; Sekar, C. Temperature Modulated Cu-MOF Based Gas Sensor with Dual Selectivity to Acetone and NO_2 at Low Operating Temperatures. *Sens. Actuators B Chem.* **2021**, *329*, 129053. [CrossRef]
29. Wei, Q.; Sun, J.; Song, P.; Li, J.; Yang, Z.X.; Wang, Q. Spindle-like $Fe_2O_3/ZnFe_2O_4$ Porous Nanocomposites Derived from Metal-Organic Frameworks with Excellent Sensing Performance Towards Triethylamine. *Sens. Actuators B Chem.* **2020**, *317*, 128205. [CrossRef]
30. Qin, W.B.; Yuan, Z.Y.; Gao, H.L.; Zhang, R.Z.; Meng, F.L. Perovskite-Structured $LaCoO_3$ Modified ZnO Gas Sensor and Investigation on Its Gas Sensing Mechanism by First Principle. *Sens. Actuators B Chem.* **2021**, *341*, 130015. [CrossRef]
31. Zhou, Q.; Zeng, W.; Chen, W.G.; Xu, L.N.; Kumar, R.; Umar, A. High Sensitive and Low-Concentration Sulfur Dioxide (SO_2) Gas Sensor Application of Heterostructure NiO-ZnO Nanodisks. *Sens. Actuators B Chem.* **2019**, *298*, 126870. [CrossRef]
32. Chang, X.; Li, X.F.; Qiao, X.R.; Li, K.; Xiong, Y.; Li, X.; Guo, T.C.; Zhu, L.; Xue, Q.Z. Metal-Organic Frameworks Derived $ZnO@MoS_2$ Nanosheets Core/Shell Heterojunctions for ppb-Level Acetone Detection: Ultra-Fast Response and Recovery. *Sens. Actuators B Chem.* **2020**, *304*, 127430. [CrossRef]
33. Zhan, M.M.; Ge, C.X.; Hussain, S.; Alkorbi, A.S.; Alsaiari, R.; Alhemiary, N.A.; Qiao, G.J.; Liu, G.W. Enhanced No_2 Gas-Sensing Performance by Core-Shell SnO_2/ZIF-8 Nanospheres. *Chemosphere* **2022**, *291*, 132842. [CrossRef] [PubMed]
34. Fan, X.X.; Xu, Y.J.; Ma, C.Y.; He, W.M. In-Situ Growth of Co_3O_4 Nanoparticles Based on Electrospray for an Acetone Gas Sensor. *J. Alloys Compd.* **2021**, *854*, 157234. [CrossRef]
35. Fan, X.X.; Wang, J.F.; Sun, C.L.; Huang, C.; Lu, Y.J.; Dai, P.; Xu, Y.J.; He, W.M. Effect of Pr/Zn on the Anti-Humidity and Acetone-Sensing Properties of Co_3O_4 Prepared by Electrospray. *RSC Adv.* **2022**, *12*, 19384–19393. [CrossRef]
36. Fan, X.-X.; He, X.-L.; Li, J.-P.; Gao, X.-G.; Jia, J. Ethanol Sensing Properties of Hierarchical SnO_2 Fibers Fabricated with Electrospun Polyvinylpyrrolidone Template. *Vacuum* **2016**, *128*, 112–117. [CrossRef]
37. Xiong, Y.; Xu, W.-W.; Zhu, Z.Y.; Xue, Q.Z.; Lu, W.B.; Ding, D.G.; Zhu, L. ZIF-Derived Porous ZnO-Co_3O_4 Hollow Polyhedrons Heterostructure with Highly Enhanced Ethanol Detection Performance. *Sens. Actuators B Chem.* **2017**, *253*, 523–532. [CrossRef]
38. Qu, F.D.; Thomas, T.; Zhang, B.X.; Zhou, X.-X.; Zhang, S.D.; Ruan, S.P.; Yang, M.H. Self-Sacrificing Templated Formation of $Co_3O_4/ZnCo_2O_4$ Composite Hollow Nanostructures for Highly Sensitive Detecting Acetone Vapor. *Sens. Actuators B Chem.* **2018**, *273*, 1202–1210. [CrossRef]
39. Cheng, P.F.; Lv, L.; Wang, Y.L.; Zhang, B.; Zhang, Y.; Zhang, Y.Q.; Lei, Z.H.; Xu, L.P. $SnO_2/ZnSnO_3$ Double-Shelled Hollow Microspheres Based High-Performance Acetone Gas Sensor. *Sens. Actuators B Chem.* **2021**, *332*, 129212. [CrossRef]
40. Lee, J.; Choi, Y.; Park, B.J.; Han, J.W.; Lee, H.-S.; Park, J.H.; Lee, W. Precise Control of Surface Oxygen Vacancies in ZnO Nanoparticles for Extremely High Acetone Sensing Response. *J. Adv. Ceram.* **2022**, *11*, 769–783. [CrossRef]
41. Reddeppa, M.; Park, B.-G.; Murali, G.; Choi, S.H.; Chinh, N.D.; Kim, D.; Yang, W.; Kim, M.-D. NO_x Gas Sensors Based on Layer-Transferred N-MoS_2/P-GaN Heterojunction at Room Temperature: Study of UV Light Illuminations and Humidity. *Sens. Actuators B Chem.* **2020**, *308*, 127700. [CrossRef]
42. Wang, S.M.; Cao, J.; Cui, W.; Fan, L.L.; Li, X.; Li, D.J.; Zhang, T. One-Dimensional Porous Co_3O_4 Rectangular Rods for Enhanced Acetone Gas Sensing Properties. *Sens. Actuators B Chem.* **2019**, *297*, 126746. [CrossRef]
43. Xu, K.; Zhao, W.; Yu, X.; Duan, S.L.; Zeng, W. MOF-Derived Co_3O_4/Fe_2O_3 PN Hollow Cubes for Improved Acetone Sensing Characteristics. *Phys. E* **2020**, *118*, 113869. [CrossRef]
44. Qu, F.D.; Jiang, H.F.; Yang, M.H. MOF-Derived $Co_3O_4/NiCo_2O_4$ Double-Shelled Nanocages with Excellent Gas Sensing Properties. *Mater. Lett.* **2017**, *190*, 75–78. [CrossRef]
45. Koo, W.-T.; Yu, S.; Choi, S.-J.; Jang, J.-S.; Cheong, J.Y.; Kim, I.-D. Nanoscale PdO Catalyst Functionalized Co_3O_4 Hollow Nanocages Using MOF Templates for Selective Detection of Acetone Molecules in Exhaled Breath. *ACS Appl. Mater. Interfaces* **2017**, *9*, 8201–8210. [CrossRef] [PubMed]
46. Xu, K.; Zhao, W.; Yu, X.; Duan, S.L.; Zeng, W. Enhanced Ethanol Sensing Performance Using Co_3O_4–$ZnSnO_3$ Arrays Prepared on Alumina Substrates. *Phys. E* **2020**, *117*, 113825. [CrossRef]
47. Li, P.P.; Jin, H.Q.; Yu, J.; Chen, W.M.; Zhao, R.Q.; Cao, C.Y.; Song, W.G. NO_2 Sensing with CdS Nanowires at Room Temperature under Green Light Illumination. *Mater. Futures* **2022**, *1*, 025303. [CrossRef]
48. Srirattanapibul, S.; Nakarungsee, P.; Issro, C.; Tang, I.-M.; Thongmee, S. Enhanced Room Temperature NH_3 Sensing of rGO/Co_3O_4 Nanocomposites. *Mater. Chem. Phys.* **2021**, *272*, 125033. [CrossRef]
49. Kim, H.-J.; Lee, J.-H. Highly Sensitive and Selective Gas Sensors Using P-Type Oxide Semiconductors: Overview. *Sens. Actuators B Chem.* **2014**, *192*, 607–627. [CrossRef]